coatings

MDPI

Article

Studying the Crucial Physical Characteristics Related to Surface Roughness and Magnetic Domain Structure in CoFeSm Thin Films

Chi-Lon Fern [1], Wen-Jen Liu [2], Yung-Huang Chang [3], Chia-Chin Chiang [4], Jian-Xin Lai [5], Yuan-Tsung Chen [5,*], Wei-Guan Chen [5], Te-Ho Wu [5], Shih-Hung Lin [6] and Ko-Wei Lin [1]

[1] Department of Materials Science and Engineering, National Chung Hsing University, Taichung 40227, Taiwan; fengcl@yuntech.edu.tw (C.-L.F.); kwlin@dragon.nchu.edu.tw (K.-W.L.)
[2] Department of Materials Science and Engineering, I-Shou University, Kaohsiung 84001, Taiwan; jurgen@isu.edu.tw
[3] Bachelor Program in Industrial Technology, National Yunlin University of Science and Technology, 123 University Road, Section 3, Douliou, Yunlin 64002, Taiwan; changyhu@yuntech.edu.tw
[4] Department of Mechanical Engineering, National Kaohsiung University of Science and Technology, Kaohsiung 80778, Taiwan; ccchiang@nkust.edu.tw
[5] Graduate School of Materials Science, National Yunlin University of Science and Technology, 123 University Road, Section 3, Douliou, Yunlin 64002, Taiwan; jianxin19971124@hotmail.com (J.-X.L.); m11147003@gemail.yuntech.edu.tw (W.-G.C.); wuth@yuntech.edu.tw (T.-H.W.)
[6] Department of Electronic Engineering, National Yunlin University of Science and Technology, 123 University Road, Section 3, Douliou, Yunlin 64002, Taiwan; isshokenmei@yuntech.edu.tw
* Correspondence: ytchen@yuntech.edu.tw; Tel.: +886-5-534-2601

Abstract: This study investigated the effects of varying film thicknesses and annealing temperatures on the surface roughness and magnetic domain structure of CoFeSm thin films. The results revealed that as the film thickness increased, both the crystalline size and surface roughness decreased, leading to a reduction in coercivity (H_c) and improved magnetic contrast performance. Energy-dispersive X-ray spectroscopy (EDS) analysis confirmed the presence of cobalt (Co), iron (Fe), and samarium (Sm) within the thin films. Notably, the 40 nm $Co_{40}Fe_{40}Sm_{20}$ thin film annealed at 200 °C exhibited lower sheet resistance (R_s) and resistivity (ρ), indicating higher conductivity and a relatively higher maximum magnetic susceptibility (χ_{ac}) at 50 Hz. These findings suggest that these films are well suited for low-frequency magnetic components due to their increased spin sensitivity. The 40 nm $Co_{40}Fe_{40}Sm_{20}$ thin film, subjected to annealing at 200 °C, displayed a distinct stripe domain structure characterized by prominently contrasting dark and bright patterns. It exhibited the lowest H_c and the highest saturation magnetization (M_s), leading to a significant improvement in their soft magnetic properties. It is proposed that the surface roughness of the CoFeSm thin films plays a crucial role in shaping the magnetic properties of these thin magnetic films.

Keywords: CoFeSm thin films; surface roughness; magnetic domain structure; electrical properties; soft magnetic properties

Citation: Fern, C.-L.; Liu, W.-J.; Chang, Y.-H.; Chiang, C.-C.; Lai, J.-X.; Chen, Y.-T.; Chen, W.-G.; Wu, T.-H.; Lin, S.-H.; Lin, K.-W. Studying the Crucial Physical Characteristics Related to Surface Roughness and Magnetic Domain Structure in CoFeSm Thin Films. *Coatings* **2023**, *13*, 1961. https://doi.org/10.3390/coatings13111961

Academic Editors: Daniela Predoi and Torsten Brezesinski

Received: 7 October 2023
Revised: 2 November 2023
Accepted: 15 November 2023
Published: 17 November 2023

1. Introduction

Spin-transfer torque magnetic random access memory (STT-MRAM) is hailed as the future of reliable magnetic random access memory (MRAM) technology, primarily due to its exceptional thermal stability, non-volatility, low write power consumption, and efficient low-current, low-frequency switching capabilities. The power consumption and overall performance of magnetic tunnel junctions (MTJs) are intricately intertwined with the composition, structure, and fabrication techniques employed for the ferromagnetic (FM) layers. Achieving cost-effective magnetization reversal hinges on the selection of soft magnetic materials featuring high saturation magnetization (M_s), elevated Curie temperature (T_c),

low coercivity (H_c), high magnetic permeability (μ), and minimal magnetostriction (λ) for the FM layer [1,2].

A memory cell for MRAM is an integration of a MTJ and a complementary metal–oxide semiconductor (CMOS) pass transistor. An MTJ is composed of an ultra-thin insulating layer and a tunnel barrier, situated between two FM metal layers [3]. Within the realm of FM materials, cobalt (Co)–iron (Fe) alloys stand out due to their high saturation magnetization (M_s), making them ideal for thin films used in read/write heads. However, it is worth noting that these alloys suffer from excessive coercivity (H_c) and insufficient corrosion resistance. The incorporation of additional elements into the CoFe alloy has the potential to enhance its soft magnetic properties and bolster its resistance to corrosion [4,5]. According to earlier studies, adding 1.7%–2.1% of vanadium (V) to CoFe alloys can provide a composition with significantly improved strength and satisfactory magnetic properties simultaneously [6]. The addition of rare earth (RE) elements in CoFe alloys is being investigated due to their electronic interaction. The interplay between the 4f-electrons of RE elements and the 3d-electrons of transition metals (TMs) through spin-orbital coupling significantly influences the electrical and magnetic characteristics of these materials [7]. Moreover, Sm^{3+} possesses five unpaired 4f electrons, potentially leading to enhancements in electrical and optical features, surface roughness, and dielectric properties [8]. Rakesh et al. investigated praseodymium (Pr)-, lanthanum (La)-, and Sm-substituted nickel–zinc (Ni-Zn) ferrite, resulting in the lattice deformation of the crystal with decreased particle size, coercivity, and magnetic exchange [9]. Furthermore, CoFe alloys with an equal composition of 50% Co and 50% Fe demonstrate remarkably high susceptibility [10]. Therefore, Sm was chosen as the alloying element to be added, and for this study, a CoFeSm alloy with a composition of 40 at. %, 40 at. %, and 20 at. % was selected.

As a third element is introduced into the parent phase, the impact of stress- and strain-induced magnetic anisotropy on material properties becomes increasingly significant. Stress–strain-induced magnetic anisotropy plays a pivotal role in determining the coercivity and practical suitability of thin films [11–13]. The findings unveil a robust and direct correlation between stress-induced magnetic anisotropy and coercivity in thin films. Under diverse stress–strain conditions, distinct alterations in the magnetic properties of the films become evident. Notably, an increase in applied stress leads to a marked enhancement of induced magnetic anisotropy, consequently resulting in a corresponding rise in coercivity [14,15]. This discovery emphasizes the central role of stress-induced magnetic anisotropy in governing the coercivity of thin films. For the sake of comprehensive analysis, we offer data on material parameters in both bulk and thin film states. The observed connection between stress-induced magnetic anisotropy and coercivity underscores the significance of mechanical stress in dictating the magnetization behavior of thin films. The application of stress induces alterations in the crystallographic orientation of magnetic domains, resulting in anisotropic characteristics. This, in turn, influences coercivity, making it more challenging for magnetic domains to reorient themselves in the presence of an external magnetic field.

In this study, $Co_{40}Fe_{40}Sm_{20}$ films of varying thicknesses and annealing temperatures were deposited on Si(100) substrates using a direct current (DC) sputtering system. The study aimed to assess how surface roughness affects the magnetic properties of $Co_{40}Fe_{40}Sm_{20}$ films, particularly in low-frequency applications. These films are known for their exceptional magnetic attributes and versatility, especially in low-frequency magnetic components. Our research sought to determine their potential in low-frequency applications and explore their low-frequency magnetic characteristics. Our experiments revealed that CoFeSm films excel in low-frequency settings, making them ideal for low-frequency magnetic components. They exhibit high low-frequency magnetic induction, with peak performance in the 50 Hz to 100 Hz range. Additionally, this work also observed variations in the film's magnetic domain structure and hysteresis loop under different thicknesses and annealing conditions, which is vital for optimizing their performance. This study

offers valuable insights for utilizing these films in low-frequency magnetic applications and serves as a valuable reference for future research and development.

2. Materials and Methods

Thin films of CoFeSm with varying film thicknesses from 10 nm to 50 nm were produced on Si(100) substrates using a DC sputtering system at room temperature (RT). The pre-cleaning steps for the Si(100) substrate are to use alcohol and then acetone for cleaning, vibrate and clean in a ultrasonic wave vibrator, and finally blow dry with nitrogen (N_2) and put it into a sputtering vacuum chamber. The composition of the alloy target of CoFeSm was 40 at. % Co, 40 at. % Fe, and 20 at. % Sm. The power density was 1.65 W/cm^2, and the deposition rate was 1.2 nm/min. The chamber base pressure was kept at 3.0 $\times$ 10^{-4} mTorr before sputtering. During sputtering, the flowing rate of argon (Ar) gas was kept at 20 sccm, the deposition power was set as 50 W, and the sputtering pressure was maintained at 3.5 $\times$ 10^{-2} mTorr. After deposition, $Co_{40}Fe_{40}Sm_{20}$ thin films were subjected to an annealing process and annealed at various temperatures up to 300 °C for 1 h with a fixed heating rate of 50 °C/min. The investigations were carried out on as-deposited films and after various annealing treatments at 100 °C, 200 °C, and 300 °C for 1 h in an Ar environment. X-ray diffraction pattern (XRD) was used to identify the crystal structure of $Co_{40}Fe_{40}Sm_{20}$ thin films. Energy dispersive X-ray spectroscopy (EDS, JEOL, Tokyo, Japan) was used to analyze the elemental composition. An atomic force microscope (AFM, NanoMagnetics Instruments, Ankara, Turkey, ezAFM) was used to investigate the surface roughness of $Co_{40}Fe_{40}Sm_{20}$ thin films. The AFM was utilized in non-contact mode, with three scanning repetitions performed at RT to ensure accurate average area assessment. Surface roughness, quantified by the arithmetic mean deviation (Ra), was determined using a scanning size of 2.5 μm $\times$ 2.5 μm. Electrical characteristics were analyzed employing a four-point probe measurement setup (Sadhudesign, Hsinchu City, Taiwan). Magnetic characteristics, including low-frequency alternating-current magnetic susceptibility (χ_{ac}), magnetic domain behavior, and hysteresis loops, were assessed using a MagQu χ_{ac} Quan II analyzer (MagQu, New Taipei City, Taiwan), magnetic force microscopy (MFM, NanoMagnetics Instruments, ezAFM), and an alternating gradient magnetometer (AGM, PMC, MicroMagTM 2900, Westerville, OH, USA), respectively. During the process of acquiring comprehensive measurements, each collected data point is determined by averaging three times.

3. Results

3.1. Structure Property and Grain Size Distribution

The XRD patterns of the as-deposited and annealed $Co_{40}Fe_{40}Sm_{20}$ thin films are illustrated in Figure 1. Distinct peaks in the X-ray diffraction (XRD) patterns are evident at specific diffraction angles (2θ) of 47.7°, 54.6°, and 56.4°, corresponding to the crystallographic planes of Co (0002), Co_2O_3 (422), and Co_2O_3 (511) [16,17]. Guojian Li et al. fabricated Co films on Si(100) substrate and observed the layer of Co films, SiO_2, and Si by transmission electron microscopy (TEM), with SiO_2 being the nature oxide for the Si substrate surface [18]. Hence, the emergence of the oxidation peak can be ascribed to the interaction of oxygen with the metal, leading to the partial oxidation of the CoFeSm thin films.

The average crystalline sizes (D) for the as-deposited and annealed $Co_{40}Fe_{40}Sm_{20}$ thin films were calculated using the Debye–Scherrer equation, as depicted in the equation below [19]:

$$D = \frac{0.9\lambda}{\beta \cos \theta_{hkl}}$$

where λ is the wavelength of the X-ray (λ = 0.154056 nm), β is the full width at half maximum (FWHM), and θ_{hkl} is the diffraction angle of the crystal plane (*hkl*).

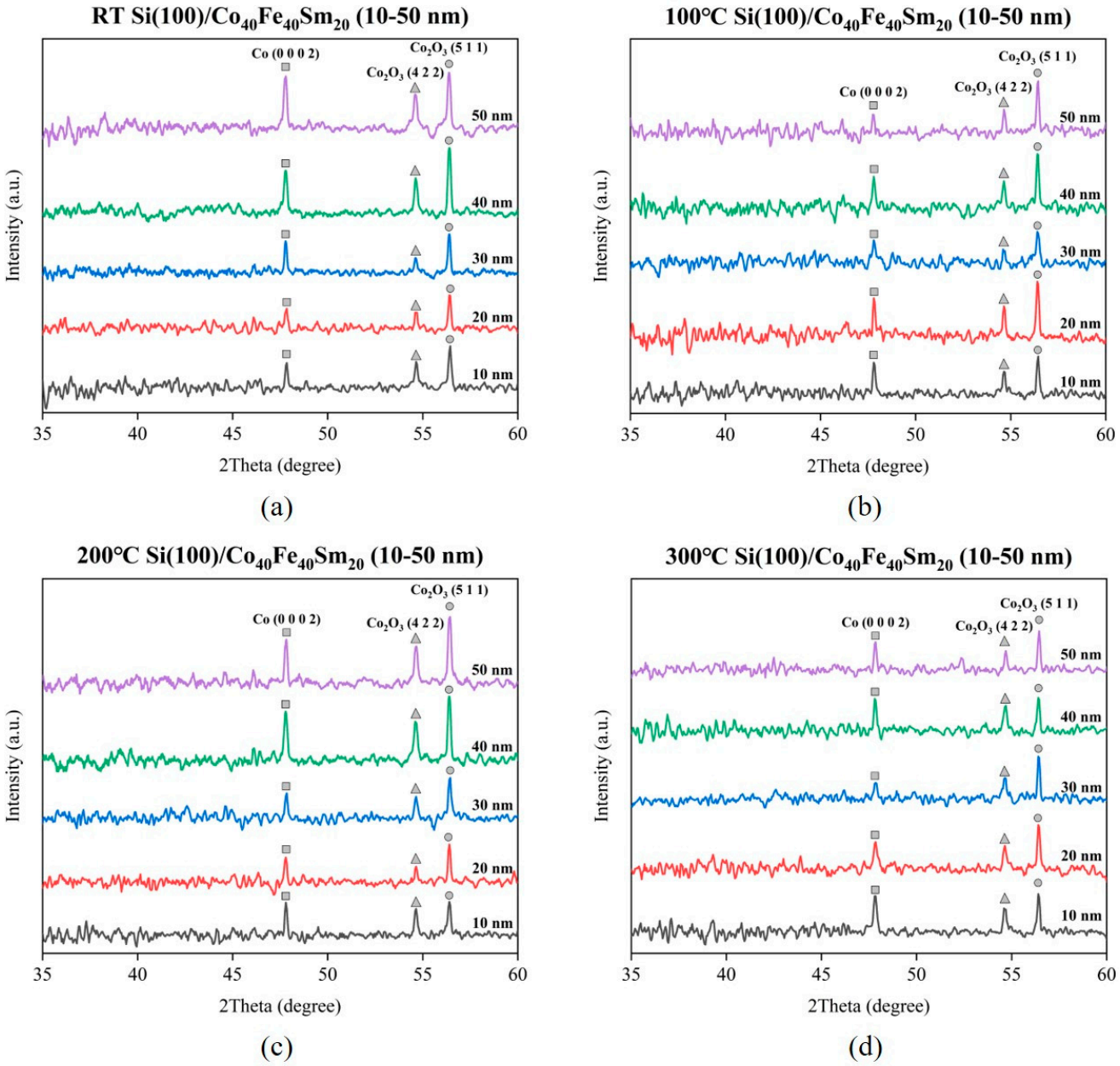

Figure 1. XRD patterns of $Co_{40}Fe_{40}Sm_{20}$ (10–50 nm) thin films with as-deposited and annealing temperatures (**a**) RT, (**b**) 100 °C, (**c**) 200 °C, and (**d**) 300 °C.

Figure 2 displays the average crystalline size of both the as-deposited and annealed $Co_{40}Fe_{40}Sm_{20}$ thin films. As the film thickness expanded from 10 nm to 50 nm and the annealing temperature rose up to 300 °C, the crystalline size of the $Co_{40}Fe_{40}Sm_{20}$ thin films notably decreased. This reduction in size resulted in the diminishment of lattice spacing in the crystallographic planes, causing compressive stress within the thin films. Moreover, the decrease in crystalline size with the escalation of film thickness and annealing temperatures can be linked to a higher rate of nucleation [20,21]. The Scherrer–Debye equation stands as a fundamental tool within the realm of crystallography, serving the purpose of ascertaining the average size of crystal grains within a material. This mathematical equation establishes a clear link between a set of parameters obtained from X-ray diffraction experiments and the dimensions of crystalline regions within the material. The connection between the Scherrer–Debye equation and experimental data is of utmost importance when it comes to characterizing the structural attributes of materials. This equation effectively associates the dimensions of crystalline regions, often referred to as crystallites, present in a material

with the observations made in X-ray diffraction patterns. The width of the diffraction peak, quantified as the FWHM, serves as an inverse indicator of crystallite size—a broader peak corresponds to smaller crystallites, and vice versa. This interplay between the Scherrer–Debye equation and experimental data entails the collection of diffraction data, typically in the form of X-ray diffraction patterns, followed by the application of the equation to determine the average size of crystallites. The strength of this correlation lies in its capability to extract structural information from a material's diffraction pattern, thereby facilitating the thorough characterization of its crystalline properties.

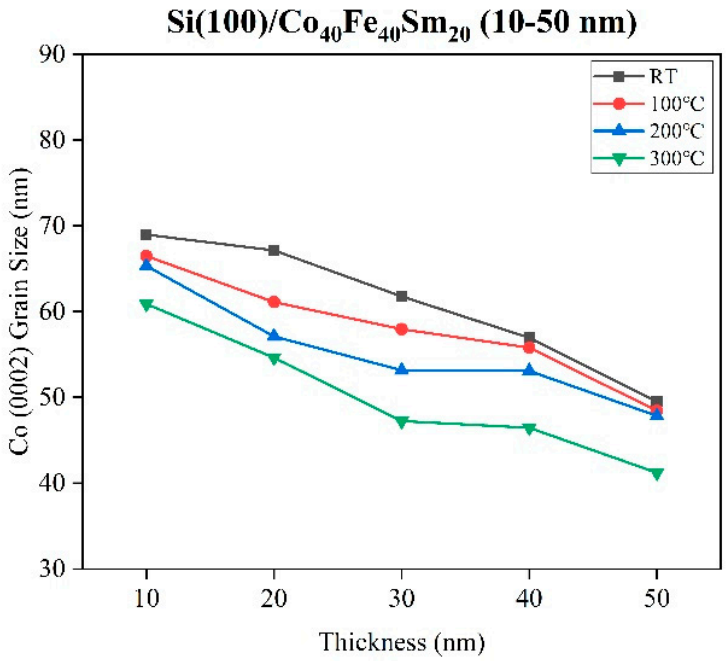

Figure 2. Average grain size of as-deposited and annealed $Co_{40}Fe_{40}Sm_{20}$ thin films with Co (0002) diffraction peak.

3.2. Composition Analysis

Figure 3 shows the pattern of energy-dispersive X-ray spectroscopy (EDS) elemental analysis for the as-deposited $Co_{40}Fe_{40}Sm_{20}$ thin films. The EDS elemental analysis confirmed the existence of Co, Fe, and Sm in the thin films. However, it was observed that the actual Co, Fe, and Sm contents did not precisely match the nominal stoichiometry of 40 at. %, 40 at. %, and 20 at. %. Nonetheless, the variation in atom content observed during film growth can be attributed to material loss incurred during the sputtering technique's transport from the target to the substrate, possibly influenced by the impact of argon ion bombardment and sputtering gun angle [22–24].

3.3. Surface Morphology and Roughness

Figure 4 illustrates the Ra values of both the as-deposited and annealed $Co_{40}Fe_{40}Sm_{20}$ thin films. For this investigation, AFM images of the as-deposited and annealed $Co_{40}Fe_{40}Sm_{20}$ thin films were scanned across an area measuring 2.5 × 2.5 μm^2. The results indicate that Ra decreased as the thickness increased. The AFM images of as-deposited and annealed 50 nm $Co_{40}Fe_{40}Sm_{20}$ thin films are displayed in Figure 5. Hence, a 50 nm thick $Co_{40}Fe_{40}Sm_{20}$ thin film annealed at 300 °C exhibited a smoother surface. This reduction in roughness can be attributed to the minimization of compressive strain and the smoothening effect caused by surface diffusion. As the annealing temperature rises, the increased energy of the atoms allows for faster migration on the substrate surface, enhancing the mobility of surface atoms and resulting in a more uniform and smoother surface. The decrease in Ra is linked to the crystalline agglomeration of the $Co_{40}Fe_{40}Sm_{20}$ thin films [25,26].

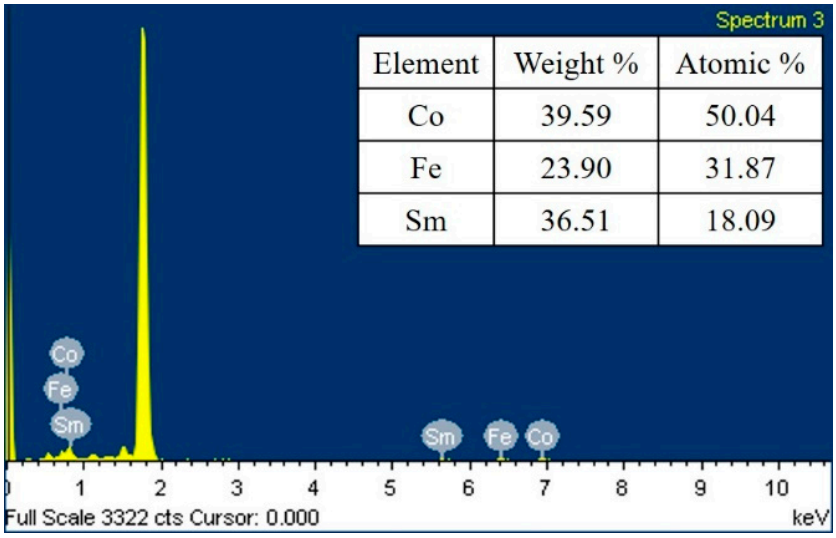

Figure 3. EDS element analysis of as-deposited $Co_{40}Fe_{40}Sm_{20}$ (40 nm) thin films.

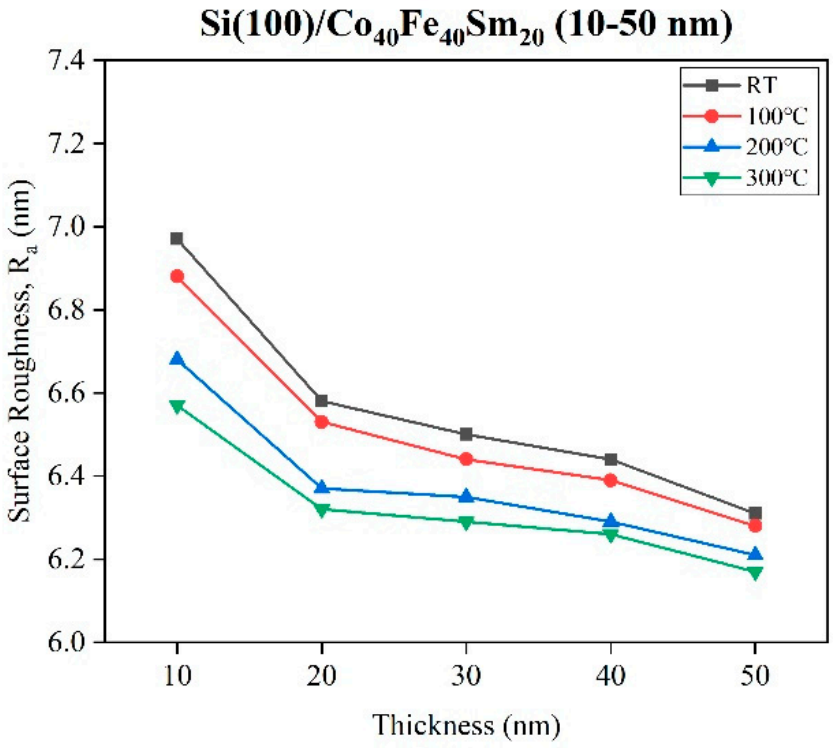

Figure 4. Surface roughness of as-deposited and annealed $Co_{40}Fe_{40}Sm_{20}$ (10–50 nm) thin films.

3.4. Electrical Characteristics

In Figure 6a,b, the sheet resistance and resistivity of both as-deposited and annealed $Co_{40}Fe_{40}Sm_{20}$ thin films are depicted. To determine the sheet resistance and resistivity values, a four-point probe instrument was used, applying a current (I) of 0.1 mA and a voltage (V) of 5 V. A drastic decreased change was found in sheet resistance and resistivity initially, but then saturated with increasing thickness. The sheet resistance and resistivity exhibited a decrease as the film thickness increased from 10 nm to 50 nm, but they decreased when the annealing temperature reached 200 °C, with a slight increase observed at 300 °C. Consequently, the annealed $Co_{40}Fe_{40}Sm_{20}$ thin films achieved their lowest sheet resistance and resistivity values at 200 °C, measuring 0.14 kΩ/sq and 0.058 × 10^{-2} Ω-cm, respectively.

The phenomenon of surface scattering becomes significant when the film thickness is comparable to the mean free path of electrons, resulting in scattering from the film's surface, and this effect diminishes as the film thickness increases, thereby boosting conductivity [27].

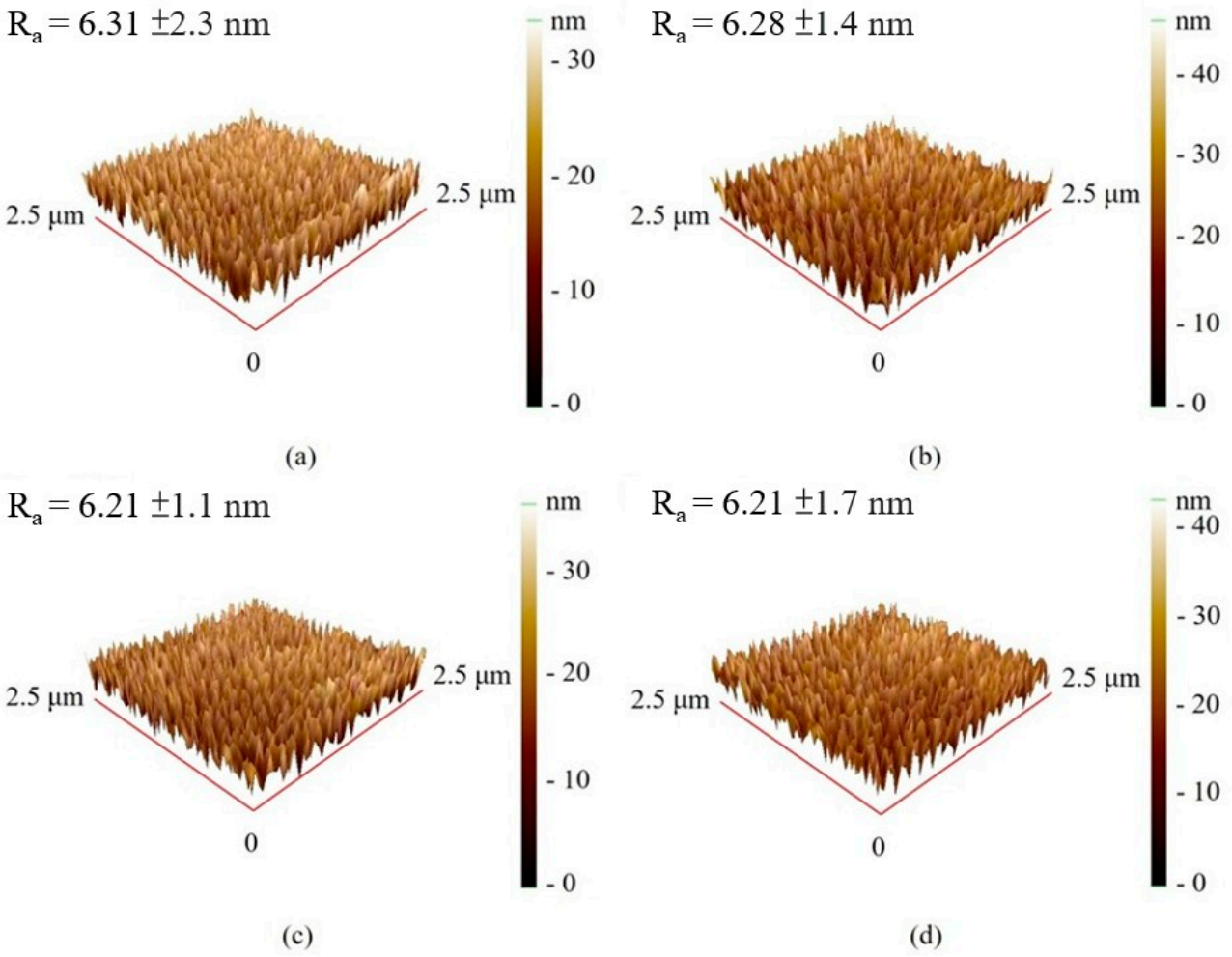

Figure 5. AFM images of 50 nm $Co_{40}Fe_{40}Sm_{20}$ thin films with different annealing temperatures: (**a**) RT, (**b**) 100 °C, (**c**) 200 °C, and (**d**) 300 °C.

Consequently, an increase in film thickness leads to a reduction in the sheet resistance and resistivity of $Co_{40}Fe_{40}Sm_{20}$ thin films.

3.5. Magnetic Properties

3.5.1. Magnetic Susceptibility

Figure 7a,b show the maximum χ_{ac} values and optimal resonance frequency of as-deposited and annealed $Co_{40}Fe_{40}Sm_{20}$ thin films. In Figure 7a, the maximum χ_{ac} demonstrates an increase with greater thickness and higher annealing temperatures. However, there was a decrease noticed at annealed 40 nm and 50 nm and 300 °C, which is likely the result of an intensified thermal disturbance effect [28]. The maximum χ_{ac} values for the as-deposited, 100 °C-annealed, and 200 °C-annealed $Co_{40}Fe_{40}Sm_{20}$ thin films were higher at 50 nm, measuring 0.11, 0.12, and 0.13, respectively. In contrast, the maximum χ_{ac} value for the 300 °C-annealed $Co_{40}Fe_{40}Sm_{20}$ thin film was higher at 30 nm, amounting to 0.13. Consequently, the 50 nm film annealed at 200 °C and the 30 nm film annealed at 300 °C exhibited the highest maximum χ_{ac} values. Prior research has suggested that higher maximum χ_{ac} values correspond to reduced motion of the free magnetic domain and heightened spin sensitivity [29]. The maximum χ_{ac} values for both the as-deposited and

annealed $Co_{40}Fe_{40}Sm_{20}$ thin films peaked within the frequency range of 50 Hz to 100 Hz. The optimal resonance frequency (f_{res}) was detected by an χ_{ac} analyzer, which means the frequency of the maximum χ_{ac}. This suggests that $Co_{40}Fe_{40}Sm_{20}$ thin films are well suited for applications in low-frequency magnetic devices such as transformers, spin valves, and magnetic recording mediums [30]. The summary of the D, Ra, Rs, ρ, maximum χ_{ac}, and optimal resonance frequency of $Co_{40}Fe_{40}Sm_{20}$ thin films subjected to various annealing temperatures is provided in Table 1.

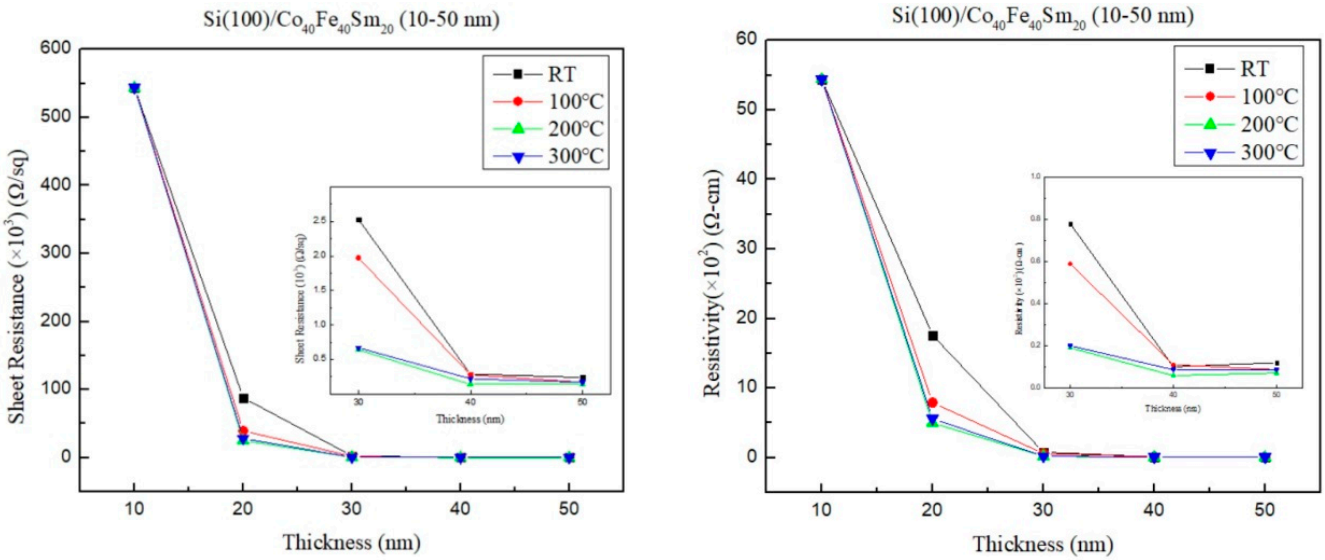

(**a**) (**b**)

Figure 6. (**a**) Sheet resistance and (**b**) resistivity of as-deposited and annealed $Co_{40}Fe_{40}Sm_{20}$ (10–50 nm) thin films.

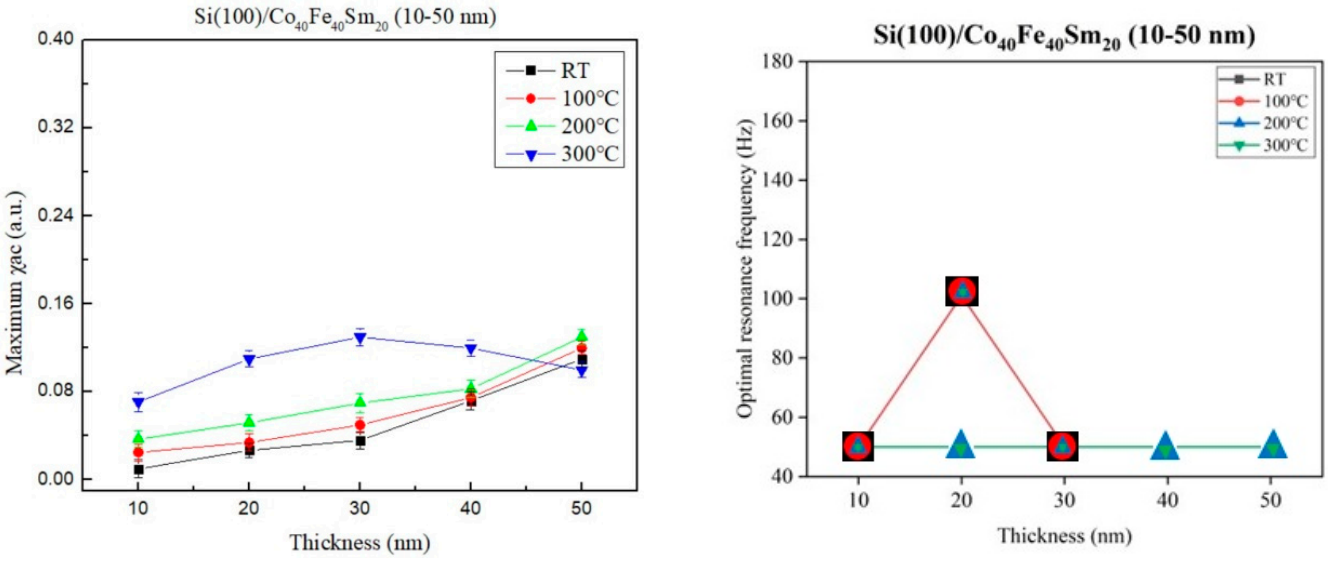

(**a**) (**b**)

Figure 7. (**a**) Maximum χ_{ac} values and (**b**) optimal resonance frequency of as-deposited and annealed $Co_{40}Fe_{40}Sm_{20}$ (10–50 nm) thin films.

Table 1. Crystalline size (*D*), surface roughness (R_a), sheet resistance (R_s), resistivity (ρ), maximum χ_{ac}, and optimal resonance frequency (f_{res}) of $Co_{40}Fe_{40}Sm_{20}$ (10–50 nm) thin films with different annealing temperatures.

T_a (°C)	Thickness (nm)	*D* (nm)	R_a (nm)	R_s (kΩ/sq)	ρ ($\times 10^{-2}$ Ω-cm)	Maximum χ_{ac} (a.u.)	Optimal Resonance Frequency (Hz)
RT	10	68.96	6.97	543.9	54.4	0.010	50
	20	67.13	6.58	87.90	17.6	0.027	100
	30	61.76	6.50	2.53	0.78	0.036	50
	40	56.95	6.44	0.29	0.10	0.072	50
	50	49.50	6.31	0.24	0.12	0.110	50
100	10	66.47	6.88	543.9	54.4	0.025	50
	20	61.10	6.53	39.36	7.87	0.034	100
	30	57.94	6.44	1.97	0.59	0.050	50
	40	55.79	6.39	0.28	0.11	0.075	50
	50	48.44	6.28	0.17	0.086	0.120	50
200	10	65.32	6.68	543.9	54.4	0.037	50
	20	57.10	6.37	25.03	5.00	0.052	50
	30	53.15	6.35	0.64	0.19	0.070	50
	40	53.08	6.29	0.14	0.058	0.083	50
	50	47.85	6.21	0.14	0.071	0.130	50
300	10	60.89	6.57	543.9	54.4	0.071	50
	20	54.62	6.32	28.05	5.61	0.110	50
	30	47.23	6.29	0.67	0.20	0.130	50
	40	46.46	6.26	0.22	0.086	0.120	50
	50	41.21	6.17	0.17	0.086	0.100	50

3.5.2. Magnetic Domain Structure

Figure 8(a1–a4) and Figure 8(b1–b4) display the MFM images of $Co_{40}Fe_{40}Sm_{20}$ thin films, specifically those with 20 nm and 40 nm thicknesses, which were subjected to different annealing temperatures. During the course of this study, MFM images of both the as-deposited and annealed $Co_{40}Fe_{40}Sm_{20}$ thin films were obtained over a scanning area measuring 10 × 10 μm^2. To prevent interference from AFM signals or Van der Waals forces, a lift height of 130 nm was employed [31]. The MFM images presented variations in contrast, with regions appearing bright, dark, and exhibiting intermediate contrast. Figure 8(a1–a4) depict the MFM images of $Co_{40}Fe_{40}Sm_{20}$ thin films with a 20 nm thickness in both the as-deposited state and after annealing. At RT, a wave stripe domain structure is evident, with the wave stripe shape growing larger upon annealing at 100 °C. However, the magnetic domain structure becomes less distinct when annealed at 200 °C and 300 °C. This observation explains the deterioration in the magnetic properties of 20 nm $Co_{40}Fe_{40}Sm_{20}$ thin films at annealing temperatures exceeding 100 °C. On the other hand, the domain structure of the 40 nm $Co_{40}Fe_{40}Sm_{20}$ thin film exhibits a particle-like pattern at RT. As the annealing temperature increases to 100 °C, the domain size expands. When annealed at 200 °C, the 40 nm $Co_{40}Fe_{40}Sm_{20}$ thin film displays a stripe domain structure with more pronounced dark and bright variations. However, at 300 °C, the magnetic properties deteriorate, resulting in ambiguous magnetic domain patterns. Consequently, magnetic contrast increases with both increasing film thickness and higher annealing temperatures due to the smoother surface. Additionally, a rougher film surface leads to a greater tip-to-sample distance, causing a decrease in magnetostatic forces and magnetic contrast [32]. While raising the annealing temperature improved the magnetic characteristics of $Co_{40}Fe_{40}Sm_{20}$ thin films, it also led to a substantial degradation at elevated annealing temperatures in films with specific 20 nm and 40 nm thicknesses. They exhibited deteriorated magnetic properties at 200 °C and 300 °C annealing temperatures, respectively. The results demonstrated that the magnetic properties of these films are significantly affected by changes in surface

characteristics and annealing conditions. Specifically, we observed that as the film thickness increased, the magnetic contrast improved, primarily due to the smoother surface promoting enhanced magnetostatic forces. On the other hand, rougher film surfaces increased the tip-to-sample distance, resulting in reduced magnetostatic forces and magnetic contrast. Additionally, our investigation revealed that the annealing process played a crucial role in altering the magnetic domain structure. While moderate annealing temperatures led to improved magnetic properties, such as larger and more distinct magnetic domains, higher annealing temperatures had a detrimental effect, leading to ambiguous or deteriorated magnetic domains. These findings underscore the importance of careful control over film thickness and annealing parameters in optimizing the magnetic properties of thin films. Further research may explore additional factors that could influence magnetic domain structure and offer a more comprehensive understanding of the underlying mechanisms. This knowledge is essential for the development and enhancement of thin film materials for various technological applications, particularly in the field of magnetic devices and data storage.

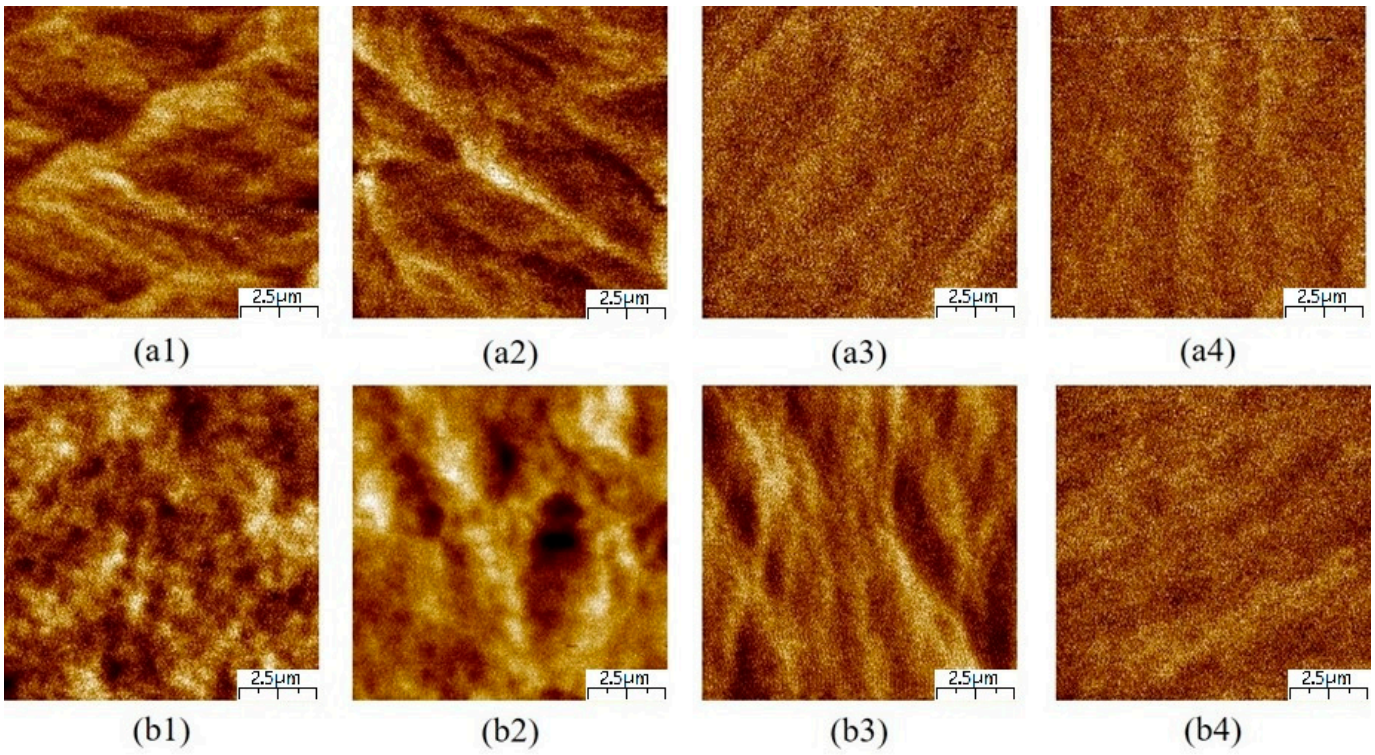

Figure 8. MFM images of 20 nm $Co_{40}Fe_{40}Sm_{20}$ thin films with annealing temperatures of (**a1**) RT, (**a2**) 100 °C, (**a3**) 200 °C, and (**a4**) 300 °C. 40 nm $Co_{40}Fe_{40}Sm_{20}$ thin films with annealing temperatures of (**b1**) RT, (**b2**) 100 °C, (**b3**) 200 °C, and (**b4**) 300 °C.

Surface roughness is a prevalent characteristic in various materials and significantly influences the behavior of magnetic domains. Understanding how surface roughness impacts the formation and behavior of magnetic domains is critical for optimizing the performance of magnetic materials. This finding reveals the considerable influence of surface roughness on the formation and properties of magnetic domains. Coarser surfaces may lead to irregular distribution of magnetic domains, while smoother surfaces could contribute to more orderly arrangements of magnetic domains [33,34]. This study highlights the close relationship between surface roughness and magnetic domains and provides valuable insights into how optimizing surface roughness can enable precise control of magnetic domains.

3.5.3. Hysteresis Loop

The $Co_{40}Fe_{40}Sm_{20}$ thin films annealed at 200 °C with a thickness of 40 nm exhibited reduced sheet resistance and resistivity, along with improved magnetic contrast. Consequently, an in-plane hysteresis loop was investigated for the 40 nm $Co_{40}Fe_{40}Sm_{20}$ thin films using AGM. Figure 9a illustrates the in-plane hysteresis loop of these thin films, and Figure 9b shows the plot of the coercivity and maximum saturation magnetization for in-plane magnetized 40 nm $Co_{40}Fe_{40}Sm_{20}$ thin films at various annealing temperatures. Table 2 presents the values of H_c, M_s, and the remanence ratio (M_r/M_s) for the 40 nm thin films at various annealing temperatures. The H_c values exhibit a decreasing trend as the annealing temperature rises, likely due to the reduction in crystalline size within the 40 nm as the annealing temperature increases from RT to 300 °C. It is worth noting that $Co_{40}Fe_{40}Sm_{20}$ thin films with finer grain structures typically display lower coercivity and adhere to a power law relationship, $Hc \propto D^6$ [5,35]. Conversely, the M_s of the 40 nm thin films increases with higher annealing temperatures, up to 200 °C, after which it decreases at 300 °C. Consequently, the 40 nm thin film annealed at 200 °C exhibits superior soft magnetic properties and is well suited for applications in spintronics, micro-actuators, magnetic memories, and storage devices. Furthermore, the 40 nm thick $Co_{40}Fe_{40}Sm_{20}$ thin film annealed at 200 °C displays a lower M_r/M_s ratio, requiring only a low demagnetization field to return to its initial magnetization state [36].

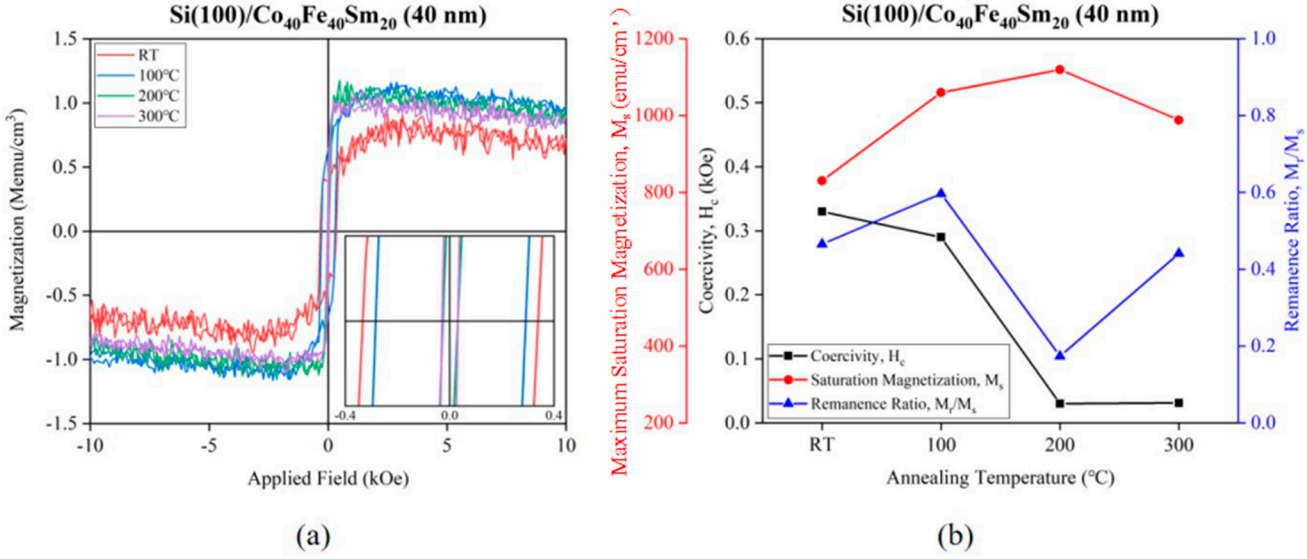

Figure 9. (**a**) In-plane hysteresis loop and (**b**) variations in coercivity, saturation magnetization, and remanence ratio for in-plane magnetization of deposited and annealed $Co_{40}Fe_{40}Sm_{20}$ (40 nm) thin films.

Table 2. Coercivity (H_c), saturation magnetization (M_s), and remanence ratio (M_r/M_s) of $Co_{40}Fe_{40}Sm_{20}$ (40 nm) thin films with different annealing temperatures (T_a).

T_a (°C)	H_c (kOe)	M_s (emu/cm^3)	M_r/M_s
RT	0.330	830.29	0.47
100	0.290	1059.82	0.60
200	0.030	1119.44	0.17
300	0.031	988.19	0.44

Taking into account the entirety of this study, the presence of oxide impurities notably impacts various physical properties of CoFeSm thin films. The exploration of how cobalt oxide (Co_2O_3) influences the magnetic and electrical characteristics of antiferromagnetic materials has become a compelling focal point in the domains of materials science and

magnetism research. Cobalt oxide possesses the capacity to exert a multifaceted influence on the properties of antiferromagnetic materials. When applied to CoFeSm thin films, cobalt oxide demonstrates the potential to modulate exchange interactions between magnetic moments and modify the materials' magnetic anisotropy, thereby influencing the orientation and stability of magnetic moments, and even decrease their overall magnetization [37]. Furthermore, the introduction of cobalt oxide impurities can induce substantial adjustments in the electrical conductivity of these materials. Consequently, this leads to variations in resistivity, refinements in conductivity mechanisms, and consequential alterations in the materials' electrical responses. It is noteworthy that the presence of oxides can obstruct the flow of electrons, resulting in electron scattering effects and an increase in the material's resistivity [38]. Recognizing the impact of cobalt oxide on the magnetic and electrical attributes of these materials is essential for tailoring their characteristics to meet specific criteria, especially in domains such as data storage, sensor technology, and emerging technological applications.

4. Conclusions

$Co_{40}Fe_{40}Sm_{20}$ thin films were manufactured on Si(100) substrates utilizing a direct current sputtering system and subsequently subjected to annealing at temperatures up to 300 °C. The investigation focused on exploring the interplay between surface roughness and the magnetic domain structure of these thin films, varying film thicknesses, and annealing temperatures. XRD analysis revealed distinct crystalline structures, notably Co (0002), Co_2O_3 (422), and Co_2O_3 (511), observed at diffraction angles of 47.7°, 54.6°, and 56.4°, respectively. EDS confirmed the presence of Co, Fe, and Sm atoms within the thin films. Notably, both the crystalline size and surface roughness decreased with escalating film thickness and higher annealing temperatures, contributing to a smoother surface. The heightened maximum χ_{ac} values denote smoother motion of free magnetic domains, suggesting increased spin sensitivity. Moreover, these films displayed their highest maximum χ_{ac} values at 50 Hz and 100 Hz, underscoring their suitability for applications in low-frequency magnetic devices. MFM revealed a more distinct stripe-like domain structure with heightened dark and bright contrasts in the 40 nm $Co_{40}Fe_{40}Sm_{20}$ thin film annealed at 200 °C. This study has provided valuable insights into the influence of various factors, including surface roughness and annealing temperature, on the magnetic domain structure of thin films. The results demonstrated that the magnetic properties of these films are significantly affected by changes in surface characteristics and annealing conditions. Specifically, we observed that as the film thickness increased, the magnetic contrast improved, primarily due to the smoother surface promoting enhanced magnetostatic forces. On the other hand, rougher film surfaces increased the tip-to-sample distance, resulting in reduced magnetostatic forces and magnetic contrast. Additionally, our investigation revealed that the annealing process played a crucial role in altering the magnetic domain structure. While moderate annealing temperatures led to improved magnetic properties, such as larger and more distinct magnetic domains, higher annealing temperatures had a detrimental effect, leading to ambiguous or deteriorated magnetic domains. The 40 nm $Co_{40}Fe_{40}Sm_{20}$ thin film annealed at 200 °C displayed the H_c and the highest M_s, highlighting their enhanced soft magnetic characteristics. Consequently, this study underscores the significant influence of surface morphology on the modulation of magnetic properties within $Co_{40}Fe_{40}Sm_{20}$ thin films.

Author Contributions: Conceptualization, C.-L.F., W.-J.L., Y.-H.C., Y.-T.C. and S.-H.L.; methodology, C.-L.F., Y.-T.C., Y.-H.C., J.-X.L., W.-G.C. and K.-W.L.; validation and formal analysis, J.-X.L., Y.-T.C. and W.-G.C.; investigation, C.-L.F., Y.-T.C. and W.-J.L.; resources, C.-C.C., T.-H.W. and K.-W.L.; writing—original draft preparation, Y.-T.C.; writing—review and editing, C.-L.F., Y.-T.C. and W.-J.L.; supervision, Y.-T.C. and Y.-H.C.; project administration, Y.-T.C., T.-H.W., and S.-H.L.; funding acquisition, C.-L.F., Y.-H.C. and C.-C.C. All authors have read and agreed to the published version of the manuscript.

Funding: This work was supported by the National Science Council, under Grant Nos. MOST 110-2221-E-992-054 -MY3, MOST108-2221-E-224-015-MY3, MOST105-2112-M-224-001, and National Yunlin University of Science and Technology, under Grant Nos. 111T01 and 113T01.

Institutional Review Board Statement: Not applicable.

Informed Consent Statement: Not applicable.

Data Availability Statement: Data are contained within the article.

Conflicts of Interest: The authors declare that there is no conflict of interest regarding the publication of this paper. The funders had no role in the design of the study; in the collection, analyses, or interpretation of data; in the writing of the manuscript; or in the decision to publish the results.

References

1. Seo, Y.; Kwen, K.W. High-density 1R/1W dual-port spin-transfer torque MRAM. *Micromachines* **2022**, *13*, 2224. [CrossRef] [PubMed]
2. Tey, M.S.V.; Chen, X.; Soumyanarayanan, A.; Ho, P. Chiral spin textures for next-generation memory and unconventional computing. *CS Appl. Electron. Mater.* **2022**, *4*, 5088–5097. [CrossRef]
3. Wolf, S.A.; Awschalom, D.D.; Buhrman, R.A.; Daughton, J.M.; Molnar, S.V.; Roukes, M.L.; Chtchelkanova, A.Y.; Treger, D.M. Spintronics: A spin-based electronics vision for the future. *Science* **2001**, *294*, 1488–1495. [CrossRef] [PubMed]
4. Kalu, E.E.; Bell, R.; Dupree, M. Improvement of the corrosion behavior of electrodeposited CoFeCu thin films. *Mater. Chem. Phys.* **2010**, *124*, 689–693. [CrossRef]
5. Mehriz, S.; Sohi, M.H.; Ebrahimi, S.A.S. Study of microstructure and magnetic properties of electrodeposited nanocrystalline CoFeNiCu thin films. *Surf. Coat. Technol.* **2011**, *205*, 4757–4763. [CrossRef]
6. George, E.P.; Gubbi, A.N.; Baker, I.; Robertson, L. Mechanical properties of soft magnetic FeCo alloys. *Mater. Sci. Eng. A* **2002**, *329–331*, 325–333. [CrossRef]
7. Tijerina-Rosa, A.; Greneche, J.M.; Fuentes, A.F.; Rodriguez-Hernandez, J.; Menéndez, J.L.; Rodríguez-González, F.J.; Montemayor, S.M. Partial substitution of cobalt by rare-earths (Gd or Sm) in cobalt ferrite: Effect on its microstructure and magnetic properties. *Ceram. Int.* **2019**, *45*, 22920–22929. [CrossRef]
8. Anwar, M.; Kayani, Z.N.; Hassan, A.; Riaz, S.; Naseem, S. Managing the micro-structure and properties of Sm-ZnO thin films by tuning the contents of Sm. *Phys. B Condes. Matter* **2023**, *662*, 414964. [CrossRef]
9. Singh, R.K.; Shah, J.; Kotnala, R.K. Magnetic and dielectric properties of rare earth substituted $Ni_{0.5}Zn_{0.5}Fe_{1.95}R_{0.05}O_4$ (R = Pr, Sm and La) ferrite nanoparticles. *Mater. Sci. Eng. B* **2016**, *210*, 64–69. [CrossRef]
10. Chotibhawaris, T.; Luangvaranunt, T.; Jantaratana, P.; Boonyongmaneerat, Y. Effects of thermal annealing on microstructure and magnetic properties of electrodeposited Co-Fe alloys. *Intermetallics* **2018**, *93*, 323–328. [CrossRef]
11. Ota, S.; Hibino, Y.; Bang, D.; Awano, H.; Kozeki, T.; Akamine, H.; Fujii, T.; Namazu, T.; Takenobu, T.; Koyama, T.; et al. Strain-induced reversible modulation of the magnetic anisotropy in perpendicularly magnetized metals deposited on a flexible substrate. *Appl. Phys. Express* **2016**, *9*, 043004. [CrossRef]
12. Miguel, C.; Zhukov, A.; González, J. Stress and/or field induced magnetic anisotropy in the amorphous $Fe_{73.5}Cu_1Nb_3Si_{15.5}B_7$ Alloy: Influence on the coercivity, saturation magnetostriction and magneto-impedance response. *Phys. Status Solidi* **2002**, *194*, 291–303. [CrossRef]
13. Leon, P.C.; Zhukova, V.; Blanco, J.M.; Legarreta, L.G.; Ipatov, M.; Zhukov, A. Stress-induced magnetic anisotropy enabling engineering of magnetic softness of Fe-rich amorphous microwires. *J. Magn. Magn. Mater.* **2020**, *510*, 166939. [CrossRef]
14. Miguel, C.L.D.; Zhukov, A.; Val, J.J.D.; González, J. Coercivity and induced magnetic anisotropy by stress and/or field annealing in Fe- and Co- based (Finemet-type) amorphous alloys. *J. Magn. Magn. Mater.* **2005**, *294*, 245–251. [CrossRef]
15. León, P.C.; Blanco, J.M.; Zhukova, V.; Ipatov, M.; Gonzalez, J.; Churyukanova, M.; Taskaev, S.; Zhukov, A. Engineering of magnetic softness and domain wall dynamics of Fe-rich amorphous microwires by stress-induced magnetic anisotropy. *Sci. Rep.* **2019**, *9*, 1247.
16. Novaković, M.; Popović, M.; Rajić, V. Study on the structural and magnetic properties of e-beam evaporated Co thin films annealed in vacuum. *J. Alloys Compd.* **2023**, *937*, 168411. [CrossRef]
17. Liu, W.J.; Chang, Y.H.; Chen, Y.T.; Jhou, T.Y.; Chen, Y.H.; Wu, T.H.; Chi, P.W. Impact of annealing on magnetic properties and structure of $Co_{40}Fe_{40}W_{20}$ thin films on Si(100) Substrate. *Materials* **2021**, *14*, 3017. [CrossRef]
18. Li, G.; Du, J.; Wang, H.; Wang, Q.; Ma, Y.; He, J. High magnetic field induced pillar growth and subsequent magnetic properties of the thermal evaporated Co thin films. *Mater. Lett.* **2014**, *133*, 53–56. [CrossRef]
19. Cullity, B.D. *Elements of X-Ray Diffraction*, 2nd ed.; Addison-Wesley: Reading, MA, USA, 1978.
20. Phua, L.X.; Phuoc, N.N.; Ong, C.K. Influence of field-annealing on the microstructure, magnetic and microwave properties of electrodeposited $Co_{0.3}Fe_{0.7}$ films. *J. Alloys Compd.* **2013**, *553*, 146–151. [CrossRef]
21. Mehrizi, S.; Molaei, M.J.; Sohi, M.H. An investigation on magnetic properties and electrical resistivity of nanocrystalline CoFeNi thick films synthesized through stabilized bath. *J. Mater. Res. Technol.* **2022**, *21*, 2547–2554. [CrossRef]

22. Vasiliev, M.; Alam, M.N.E.; Alameh, K.; Premchander, P.; Lee, Y.T.; Kotov, V.A.; Lee, Y.P. Annealing behaviour and crystal structure of RF-sputtered Bi-substituted dysprosium iron-garnet films having excess co-sputtered Bi-oxide content. *J. Phys. D Appl. Phys.* **2011**, *44*, 075002. [CrossRef]
23. Sundberg, J.; Lindblad, R.; Gorgoi, M.; Rensmo, H.; Jansson, U.; Lindblad, A. Understanding the effects of sputter damage in W–S thin films by HAXPES. *Appl. Surf. Sci.* **2014**, *305*, 203–213. [CrossRef]
24. Achenbach, J.O.; Mraz, S.; Primetzhofer, D.; Schneider, J.M. Correlative experimental and theoretical investigation of the angle-resolved composition evolution of thin films sputtered from a compound Mo_2BC target. *Coatings* **2019**, *9*, 206. [CrossRef]
25. Cao, Y.; Zhou, C. Thickness dependence of surface roughness and magnetic properties of FeNiCr thin films. *J. Magn. Magn. Mater.* **2013**, *333*, 1–7. [CrossRef]
26. Biswal, S.R.; Kar, J.P. Effect on electrical properties of CuI thin film prepared by a spin coating technique. *Mater. Today Proc.* **2023**, *76*, 403–405. [CrossRef]
27. Khojier, K.; Savaloni, H. A study on the dependence of DC electrical properties and nanostructure of Cu thin films on film thickness. *Int. J. Nano Dimens.* **2013**, *3*, 217–226.
28. Sousa, W.J.; Guerra, Y.; Garcia, P.; Hernández, E.P. Saturation magnetization as a function of temperature in Zn doped YIG nanoparticles. *Phys. E Low-Dimens. Syst. Nanostruct.* **2022**, *138*, 115054. [CrossRef]
29. Chen, Y.T.; Chang, Z.G. Low-frequency alternative-current magnetic susceptibility of amorphous and nanocrystalline $Co_{60}Fe_{20}B_{20}$ films. *J. Magn. Magn. Mater.* **2012**, *324*, 2224–2226. [CrossRef]
30. Chen, Y.T.; Chang, Y.H.; Liu, W.J.; Liang, W.C.; Hsieh, C.H.; Wu, T.H. Effect of low-frequency AC magnetic susceptibility of $Ru/Co_{60}Fe_{20}V_{20}$ and $Ta/Co_{60}Fe_{20}V_{20}$ films. *J. Magn. Magn. Mater.* **2018**, *465*, 651–653. [CrossRef]
31. Porthun, S.; Abelmann, L.; Lodder, C. Magnetic force microscopy of thin film media for high density magnetic recording. *J. Magn. Magn. Mater.* **1998**, *182*, 238–273. [CrossRef]
32. Göddenhenrich, T.; Lemke, H.; Hartmann, U.; Heiden, C. Magnetic force microscopy of domain wall stray fields on single crystal iron whiskers. *Appl. Phys. Lett.* **1990**, *56*, 2578–2580. [CrossRef]
33. Swerts, J.; Vandezande, S.; Temst, K.; Haesendonck, C.V. Surface roughness effects on the magnetization reversal of polycrystalline Fe/Ag thin films. *Solid State Commun.* **2004**, *131*, 359–363. [CrossRef]
34. Zhao, Y.; Gamache, R.; Wang, G.C.; Lu, T.M.; Palasantzas, G.; Hosson, J.T.M.D. Effect of surface roughness on magnetic domain wall thickness, domain size, and coercivity. *J. Appl. Phys.* **2001**, *89*, 1325–1330. [CrossRef]
35. Bolyachkin, A.S.; Komogortsev, S.V. Power-law behavior of coercivity in nanocrystalline magnetic alloys with grain-size distribution. *Scr. Mater.* **2018**, *152*, 55–58. [CrossRef]
36. Zan, F.L.; Ma, Y.Q.; Ma, Q.; Zheng, G.H.; Dai, Z.X.; Wu, M.Z.; Li, G.; Sun, Z.Q.; Chen, X.S. One-step hydrothermal synthesis and characterization of high magnetization $CoFe_2O_4/Co_{0.7}Fe_{0.3}$ nanocomposite permanent magnets. *J. Alloys Compd.* **2013**, *553*, 79–85. [CrossRef]
37. Thibodeaux, C.A.; Kulkarni, V.; Chang, W.S.; Neumann, O.; Cao, Y.; Brinson, B.; Orozco, C.A.; Chen, C.W.; Morosan, E.; Link, S.; et al. Impurity-induced plasmon damping in individual cobalt-doped hollow Au nanoshells. *J. Phys. Chem. B* **2014**, *118*, 14056–14061.
38. Jud, E.; Gauckler, L.J. The Effect of Cobalt Oxide Addition on the Conductivity of $Ce_{0.9}Gd_{0.1}O_{1.95}$. *J. Electroceramics* **2005**, *15*, 159–166. [CrossRef]